Complex Formation of Gold Nanoparticles with Collagen in Aqueous Media Studied by X-ray Scattering and Absorption Spectroscopy

Kota Sagawa, Ken Terao*

Department of Macromolecular Science, Graduate School of Science, Osaka University, 1-1, Machikaneyama-cho, Toyonaka, Osaka 560-0043, Japan

* Corresponding author. Tel.: +81 6 6850 5461.

E-mail address: terao.ken.sci@osaka-u.ac.jp (K. Terao)

ABSTRACT

Small-angle X-ray scattering and UV-vis absorption measurements were performed on mixed solutions of gold nanoparticles (AuNPs) and atelocollagen (AC), triple-helical collagen without telopeptide, in acetate buffer at pH 4 under different temperature conditions, i.e., preparation temperature T_{prep} and measurement temperature T_{meas}. Due to the significantly higher electron density of gold than that of AC, the structure factor $S(q)$ of AuNPs is readily estimated from the scattering intensities of AuNP-only and mixed solutions. The resulting $S(q)$ profile for the mixed solution indicated significant attractive interactions, especially for the smaller AuNPs. Therefore, the sticky sphere model was applied to analyze $S(q)$ to determine the interaction parameters at different T_{prep} and T_{meas}. The attractive interactions between AuNPs were higher at higher T_{prep}, suggesting that single-chain AC tends to make the interactions between AuNPs more attractive than those for triple-helical AC. Complex formation was also detected by the aggregation-induced surface plasmon absorption shift. More densely-packed AuNPs were detected from the absorption spectra for higher AuNP content at which the ζ potential disappeared, while a split absorption band was also found, indicating that not all AuNPs can form a complex with AC at $\zeta = 0$.

INTRODCUCTION

Gold nanoparticles (AuNPs) have been widely used for biomedical applications, such as drug delivery and biosensors, because AuNPs can be readily linked to various molecules, including oligo-DNA (or DNA origami) and antibodies.[1-5] One of the significant characteristics of AuNPs is the size-dependent surface plasmon resonance which can be readily observed by visible light absorption spectra. Indeed, a number of applications as biosensors have been investigated.[6, 7] In particular, specific optical properties can be programmed by the DNA-AuNP assemblies.[8-10] Intermolecular interactions between AuNPs and various biomacromolecules are of interest for the development of novel functional nanomaterials. Among them, intermolecular interactions between AuNPs and antibody peptides have been investigated to reduce nonspecific aggregation in vivo.[11] Interaction between AuNPs and proteins is a significant issue used for biomedical applications. A number of characterizations of the complex consisting of AuNPs and proteins in aqueous media have been investigated.[12-14]

Collagen is the most abundant protein in mammals and is mainly found in connective tissues. The intermolecular interactions and complex formation between AuNPs and collagen are of interest for a proper understanding of the above-mentioned biomedical applications of AuNPs. However, they have been little investigated probably due to the lower solubility of native collagen in neutral buffer solutions. On the other hand, the intermolecular interaction between AuNPs and collagen is also of interest for the synthesis of collagen hybrid AuNPs[15, 16] which have a nonspherical shape in aqueous media. Furthermore, this interaction is also used as an optical probe to detect the fiber-like aggregation of collagen.[17] The interactions are also studied in terms of molecular dynamics simulation to find the unfolding nature of collagen on the AuNPs.[18]

Recently, association behaviors of silica nanoparticles (SiNPs) in the presence of collagen[19, 20] and a double helical polysaccharide, xanthan,[21] have been studied by small angle X-ray scattering (SAXS) in aqueous buffer solutions. While scattering measurements are easily obstructed by small amounts of large aggregates, we successfully determined the interaction parameters of SiNPs in the presence of collagen when we chose an acidic buffer of pH 3 or 4 as solvent and atelocollagen (AC) instead of native collagen, i.e. AC is triple-helical collagen without nontriple helical telopeptides. Interactions between SiNPs can be influenced by the conformation of collagen. Specifically, densely packed SiNPs were observed for the single-chain collagen and negatively charged SiNPs, while relatively loosely packed SiNPs were found for the triple-helical collagen and SiNP mixture, suggesting that not only electrostatic but also hydrogen bonding interactions play an important role in the complexion.

If sufficient dispersibility is achieved for AuNP-AC systems in the same buffer, it can be a good model system to investigate intermolecular interactions between collagen and AuNPs considering the significant change in the absorption band of aggregated AuNPs in aqueous media. Furthermore, elucidation of complexation can provide important insights for controlling the 3D structure of the collagen-AuNP hybrid materials, since SAXS data give us information about the spatial structure, while surface plasmon resonance reflects neighbor interactions. As an example of combined spectroscopy and SAXS analysis, we have recently found a novel intermediate state for the double helical polysaccharide xanthan by combining SAXS and circular dichroism measurements.[22] In this study, SAXS and UV-vis absorption measurements were investigated for different sized AuNPs with AC, for which non-triple helical telopeptides were removed by an enzymatic reaction[23] to reveal the complex formation behavior of different sized AuNPs in the presence of triple helical or single chain AC.

EXPERIMENTAL SECTION

Samples. Reactant-free gold nanoparticles (AuNPs), AuNP-5, AuNP-10, AuNP-10′, AuNP-20, AuNP-50, and AuNP-100, with diameters of 5, 10, 10, 20, 50, and 100 nm, respectively, dispersed in 0.1 mM phosphate-buffered saline (PBS) were purchased from Merck Co., Ltd, with AuNP-10 and AuNP-10′ being the different lots. The mass concentrations c_{NP} of AuNP were 0.0694, 0.0607, 0.0531, 0.0445, and 0.0389 mg/mL for AuNP-5, AuNP-10 (AuNP-10′), AuNP-20, AuNP-50, and AuNP-100, respectively, according to the reagent data sheet. An AC sample (Koken, Japan), in which the triple-helical structure is retained and the nontriple helical telopeptides are enzymatically removed, is used for this study. AC was dissolved in 50 mM acetate buffer (pH 4), and the mass concentration c_{AC} of AC was c_{AC} = 0.010 mg/mL. Equal volumes of AuNP and AC solutions were mixed to obtain an isovolumetric mixed solution in which both c_{AC} and c_{NP} were half of the corresponding initial solution. The buffer concentration of the mixture can be considered as 25 mM and the pH as 4, since the buffer concentration of PBS in the original AuNP solution is quite low (0.1 mM). We chose this pH because it is difficult to dissolve AC at higher pH and the dispersibility of AuNP may decrease with decreasing pH. Mixed solutions with other mixing ratios were also prepared to evaluate the c_{NP}/c_{AC} dependence of some physical properties as described below. The following measurement was made on the same day as the solution was prepared because some color change and/or visible aggregation was observed after one week. For a similar system, SiNP-AC, we checked that the SAXS intensity reached an asymptotic value after 20 min of mixing.[20]

Electrophoretic Light Scattering (ELS). ELS measurements were conducted for mixed solutions of AC and AuNP using an ELSZ-2 zeta potential analyzer (Otsuka, Japan) to

determine the electrophoretic mobility u at 15 °C. The ζ potential was calculated from u in terms of the Smoluchowski equation.

Small-Angle X-ray Scattering (SAXS). SAXS measurements were made at the BL40B2 beamline in SPring-8 (Hyogo, Japan) for mixed solutions of AC and AuNPs at different preparation temperatures T_{prep} and measurement temperatures T_{meas}. The wavelength λ_0 of the incident light in a vacuum and the sample-to-detector distance were set to be 0.1 nm and 4.2 m, respectively. The scattered light was detected by using a PILATUS3 2M detector (Dectris). The magnitude q of the scattering vector at each pixel on the detector was determined from the Debye Scherrer ring pattern of silver behenate. The incident light intensity was detected at both the upper and lower sides of the cell to compensate for the scattered intensity $I(q)$, taking into account the transmittance of the X-ray. The excess scattered intensity $\Delta I(q)$ of the solution was evaluated from the numerical $I(q)$ difference between a solution and the solvent with the same buffer concentration. The SAXS measurement was also evaluated for AuNPs without AC in the same buffer of the mixed solution to evaluate the structure factor of AuNPs as described below.

UV-Vis Absorption. Absorption measurements in the λ_0 range of 300 nm to 900 nm were performed using a V-750 UV/vis spectrometer with a thermostatic cell holder. A rectangular cell with a path length of 1 mm was used. Both T_{prep} and T_{meas} were varied as in the case of the SAXS measurement.

Total Holographic Characterization.[24] A two-dimensional visible-light scattering profile was obtained using Spheryx's xSight to determine the particle size and refractive index of each particle in terms of the Lorenz-Mie theory. The measurement was conducted for the mixture of AC in acetate buffer (50 mM, pH = 4) and AuNP in 0.1 mM phosphate-buffered saline at 25 °C. The mixture was prepared at both T_{prep} = 0 °C and 50 °C.

RESULTS AND DISCUSSION

ζ-potential. Figure 1 shows the c_{AC}/c_{NP} dependence of ζ for the mixed solutions of AuNPs and AC. All AuNPs have negative ζ potential while AC has positive ζ. Isovolumetric mixtures of the two solutions of AuNPs and AC have positive ζ for AuNP-10, AuNP-20, AuNP-50, and AuNP-100 while the mixture with AuNP-5 has a negative value. Taking into consideration that the c_{NP} of the original solution is in the same order, it has a positive correlation with the surface area per weight of gold. The ζ value is mostly independent of c_{AC}/c_{NP} at high c_{AC}/c_{NP}. It decreases abruptly and becomes negative with decreasing c_{AC}/c_{NP}. The c_{AC}/c_{NP} values for the isoelectric mixture are estimated to be 0.4, 0.07, 0.03, 0.009, and 0.0045 for AuNP-5, AuNP-10, AuNP-20, AuNP-50, and AuNP-100, respectively. Assuming that both the density and the surface charge density are independent of AuNP size, the surface area of AuNP at a given constant concentration is expected to be proportional to the diameter. This relationship is mostly comparable to the current data except for the smallest AuNP, thus reasonable.

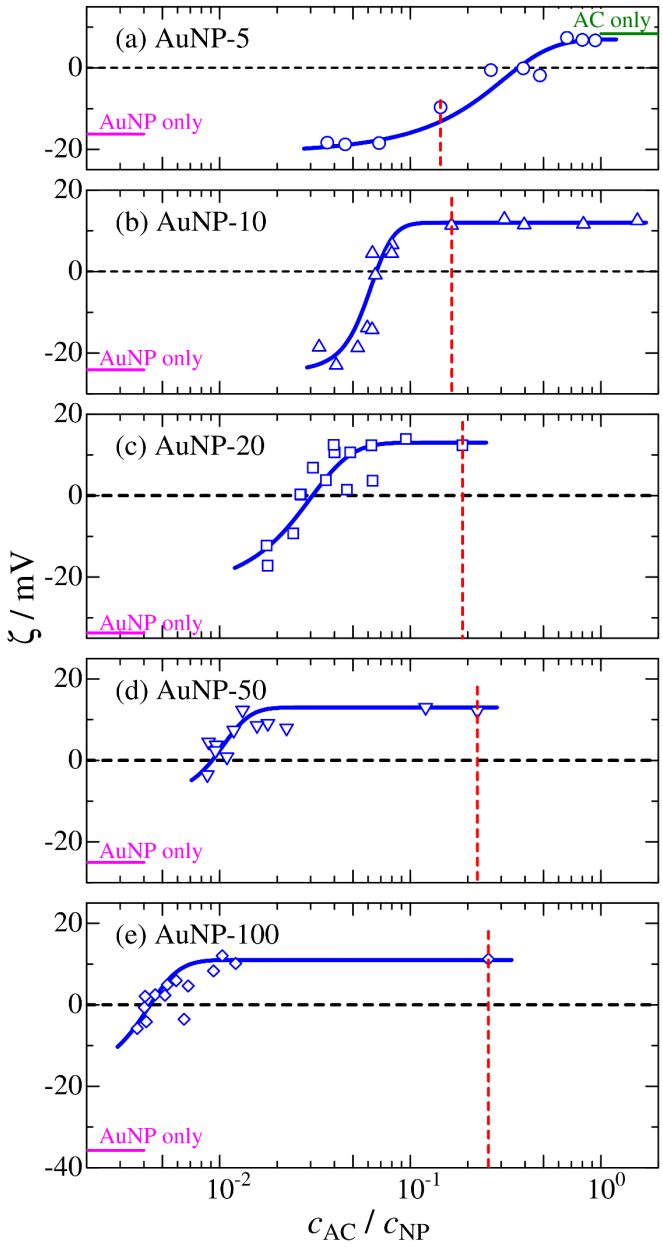

Figure 1. Composition c_{AC}/c_{NP} dependence of the ζ-potential for the mixed solutions of AC (c_{AC} = 1.0 × 10^{-2} mg/mL) in the acetate buffer (50 mM, pH = 4) and AuNPs in 0.1 mM phosphate-buffered saline at 15 °C. (a) AuNP-5, (b) AuNP-10, (c) AuNP-20, (d) AuNP-50, and (e) AuNP-100. Dashed lines indicate the isovolumetric mixture.

Size of the Complex Estimated from Holographic Characterization. It is known that the polyion complexes tend to form large droplets.[25, 26] Indeed, aggregates of visible size have been observed for the SiNP-AC complex.[19] We therefore observed the resulting droplets in the AuNP-AC mixed solution using a light scattering method (xSight). This allows us to evaluate the size and refractive index of each droplet or particle in the solution. Figure 2 is an example of the data for an isovolumetric mixed solution (positive ζ) of AuNP-10 and AC prepared at 50 °C. A number of micrometer-sized droplets were observed, suggesting that each droplet contains a large number of AC molecules and AuNPs. The results for the other systems are summarized in Figures S1 and S2 for isovolumetric (positive ζ) and $\zeta = 0$ mixtures, respectively, at two different T_{prep}. However, no significant trend and/or difference was found in the data. Since the concentration of both AuNPs and AC are significantly low, optical microscopy is not suitable for this system. It should be noted that conventional light scattering methods are difficult to apply to this system due to the significant absorption of visible light, and the emission may affect the detected data.

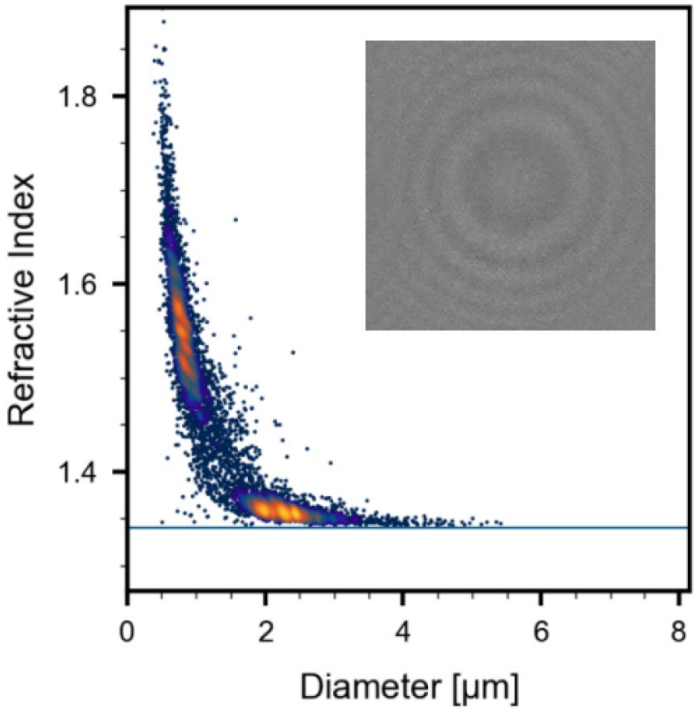

Figure 2. One example of the result from the total holographic characterization for isovolumetric mixture solution of AuNP-10 and AC prepared at 50 °C. Relationship of refractive index and diameter estimated from the scattering pattern from the particle (Inset).

Structure Factor of AuNPs. The excess scattering intensity $\Delta I(q)$ of AuNPs in 25 mM acetate buffer at 15 °C was illustrated in Figure S3. The shapes are typical for the spherical particles with a certain size dispersion. Assuming the log-normal distribution for the size dispersion, the form factor $P(q)$ proportional to $\Delta I(q)$ can be expressed as

$$P(q) = \frac{\int_0^\infty \Phi^2(qR) w(R) R^3 \mathrm{d}R}{\int_0^\infty w(R) R^3 \mathrm{d}R} \quad (1)$$

$$\Phi(x) = \frac{3(\sin x - x\cos x)}{x^3} \quad (2)$$

$$w(R) = \frac{1}{\sqrt{2\pi}\sigma_{\mathrm{R}}R}\exp\left\{-\frac{[\ln(R/R_{\mathrm{m}})]^2}{2{\sigma_{\mathrm{R}}}^2}\right\} \quad (3)$$

where R_{m} and σ_{R} are the mean radius and the radius dispersion parameter, respectively. A curve fitting procedure was employed to estimate R_{m} and σ_{R}. The resulting parameters are summarized in Table 1, and the calculated theoretical values are illustrated in Figure S3 and as green curves in Figure 3. While the mean diameter (2 R_{m}) is consistent with the data sheet and the dispersity parameter σ_{R} is in a reasonable range of 0.10 to 0.14, the $\Delta I(q)$ in the low q range for AuNP-10 and AuNP-10′ are appreciably higher than the theoretical values, suggesting that the small amount of AuNPs form aggregates in the buffer solution. It should also be noted that the significantly scattered data in Figures 3 and S3 are observed when $\Delta I(q)$ is approximately smaller than 10^{-2}, suggesting that the experimental error on $\Delta I(q)$ is on the order of 10^{-2}.

Table 1. Mean Diameter $2R_{\mathrm{m}}$ and Dispersion Parameter σ_{R} of the AuNPs in the Acetate Buffer

Sample	$2R_{\mathrm{m}}$ / nm	σ_{R}
AuNP-5	5.1 ± 0.2	0.13
AuNP-10	7.8 ± 0.2	0.10
AuNP-10′	8.6 ± 0.3	0.14
AuNP-20	19.4 ± 0.5	0.13
AuNP-50	53 ± 2	0.13
AuNP-100	100 ± 5	0.13

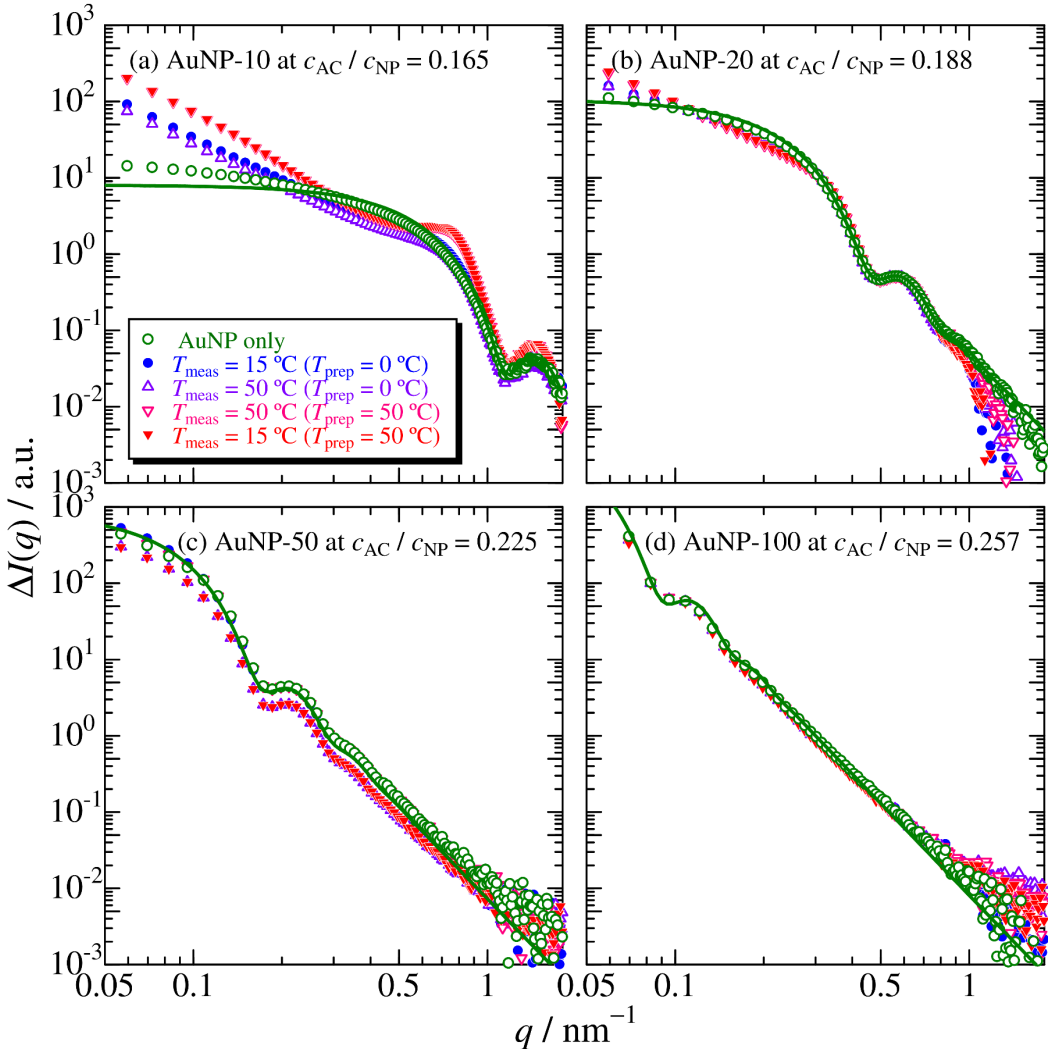

Figure 3. Double logarithmic plots of excess scattering intensity $\Delta I(q)$ vs. q for the isovolumetric mixture of AC (c_{AC} = 1.0 × 10^{-2} mg/mL) in acetate buffer (50 mM, pH = 4) and AuNP in 0.1 mM phosphate-buffered saline. (a) AuNP-10 at c_{AC}/c_{NP} = 0.165, (b) AuNP-20 at c_{AC}/c_{NP} = 0.188, (c) AuNP-50 at c_{AC}/c_{NP} = 0.225, (d) AuNP-100 at c_{AC}/c_{NP} = 0.257 at the indicated temperature conditions. The gold-only solution was prepared by isovolumetric mixing with 50 mM acetate buffer. Solid green curves indicate calculated values for polydisperse spheres (see text).

Figure 3 also illustrates the q dependence of $\Delta I(q)$ for isovolumetric mixtures of AuNP and AC solutions mixed and prepared at the indicated temperatures. It should also be noted that we showed the data for AuNP-5 in Figure S4 because the sign of ζ is different from the other mixtures and consequently the electrophoretic properties of the complex may be different from those with the other AuNPs. The temperature conditions were referred to as the preparation temperature T_{prep}, at which AC and AuNP solutions were mixed, and the measurement temperature T_{meas} of the SAXS. Four temperature conditions were attempted for each AuNP, i.e. T_{prep} = 0 and 50 °C and T_{meas} = 15 and 50 °C. It should be noted that AC forms a triple helical structure in acetate buffer at both 0 and 15 °C, while it unwinds at 50 °C but does not rewind even at 15 °C, at least for several hours.[19] We also confirmed that the scattering intensity from AC in the buffer at higher c_{AC} is comparable to the theoretical values for the molecularly dispersed AC.[19] The evaluated scattering profiles of the mixed solutions, except for AuNP-100, are different from those of AuNPs, suggesting significant aggregation of small AuNPs by collagen molecules. Another important point is that substantially the same $\Delta I(q)$ data for AuNP-100 with and without AC indicate that AC does not directly affect the scattering profile under the current experimental conditions. This is reasonable because the scattering intensity from AC was negligible in the investigated $c_{\mathrm{NP}}/c_{\mathrm{AC}}$ range as shown in the Supporting Information with Figure S5, where the calculation was verified using X-ray scattering theory[27-30] and the experimental values for collagen model peptides.[31] Thus, the apparent structure factor $S(q)_{\mathrm{app}}$ for the larger AuNPs is evaluated from the following equation as

$$S(q)_{\mathrm{app}} = \frac{\Delta I(q)_{\mathrm{mix}}}{\Delta I(q)_{\mathrm{AuNP}}} \tag{4}$$

where $\Delta I(q)_{mix}$ and $\Delta I(q)_{AuNP}$ indicate the excess scattering intensity for the mixed solution and AuNP solution, respectively, in which c_{NP}'s are identical. This equation also assumes that the form factor of AuNP in the mixed solution is the same as that in the AuNP-only solution. The resulting $S(q)_{app}$ data are plotted against q in Figure 4. If the interparticle interactions are negligible, then $S(q)_{app}$ should be unity and independent of q. Consequently, the wavelike plots for AuNP-10 and AuNP-20 clearly indicate significant attractive interparticle interactions through AC molecules, taking into account the very low c_{NP}. Some $S(q)_{app}$ data in the high q range are quite different from unity, while the structure factor $S(q)_{app}$ should converge to 1 at high q. This is most likely because the mass concentrations of AuNP in the scattering volume are different from those of c_{NP} due to the formation of the large aggregate. This is reasonable because micrometer sized droplets were observed as described above with Figures 2, S1, and S2. It should be noted that the $S(q)_{app}$ data for AuNP-10 may not be reliable in a q range below 0.2 nm^{-1} because $\Delta I(q)_{AuNP}$ for the AuNP in the q range are appreciably larger than the theoretical values for polydisperse spheres as shown in Figures S3 and 3(a).

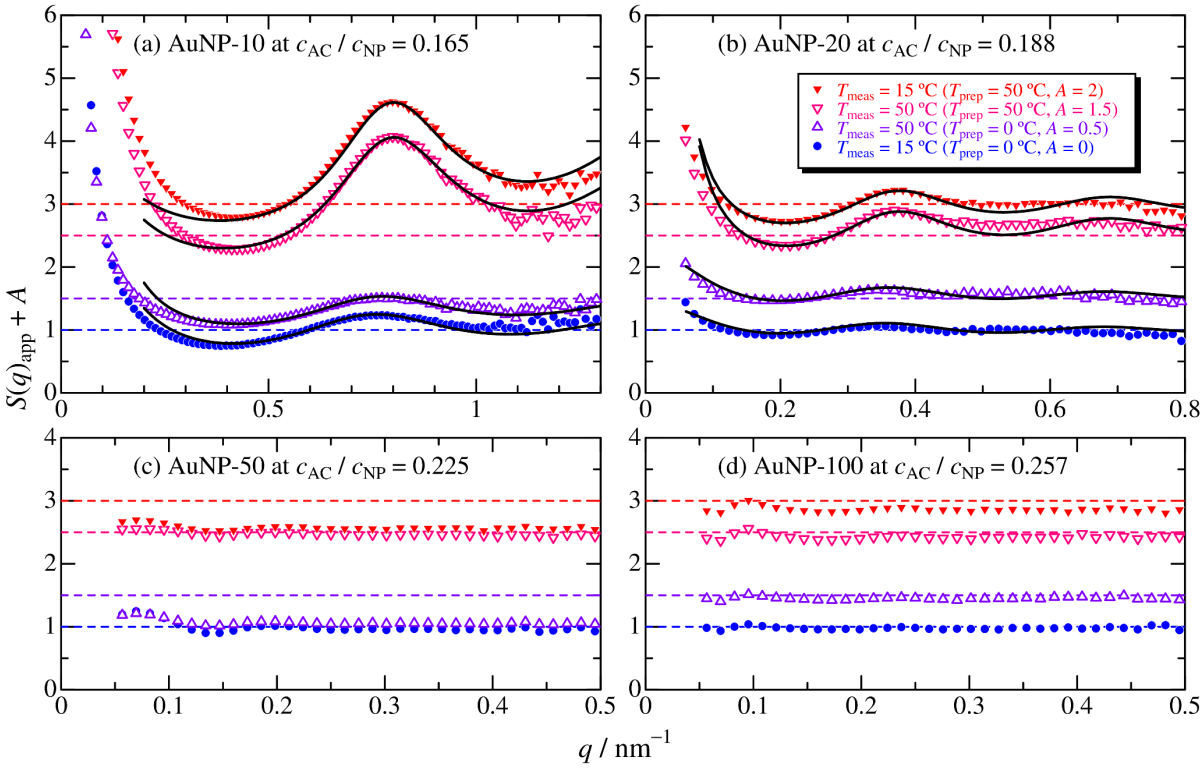

Figure 4. Plots of $S(q)$ vs q estimated for the positive ζ mixtures. (a) AuNP-10 at c_{AC}/c_{NP} = 0.165, (b) AuNP-20 at c_{AC}/c_{NP} = 0.188, (c) AuNP-50 at c_{AC}/c_{NP} = 0.225, (d) AuNP-100 at c_{AC}/c_{NP} = 0.257 at the indicated temperature conditions. Solid curves denote theoretical values with the parameters listed in Table 2. Dashed lines, $S(q)$ = 1.

Similar data treatment was also used for $\zeta = 0$ mixtures. The scattering intensity from AC is also negligible to estimate $S(q)_{app}$ because the c_{AC}/c_{NP} values are lower than those for the corresponding isovolumetric mixture as shown in Figure 4. It is also noted that the scattering intensity from AC may not be negligible for the $\zeta = 0$ mixtures for AuNP-5 because of the high c_{NP}/c_{AC} (= 0.4) as shown in Figure 1. The resulting $S(q)_{app}$ data are shown in Figure 5. At least apparently, this plot is similar to those in Figure 4, indicating significantly attractive interactions between AuNPs.

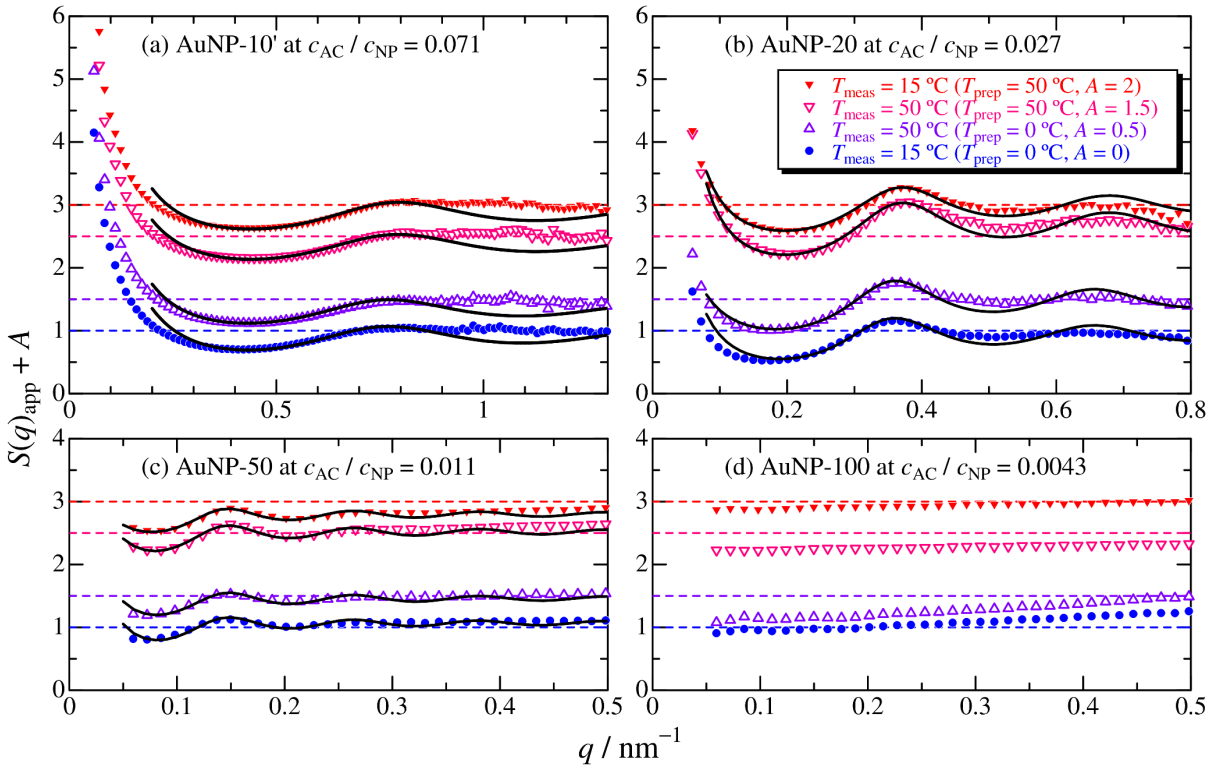

Figure 5. Plots of $S(q)$ vs q for the $\zeta = 0$ mixtures. (a) AuNP-10′ at c_{AC}/c_{NP} = 0.071, (b) AuNP-20 at c_{AC}/c_{NP} = 0.027, (c) AuNP-50 at c_{AC}/c_{NP} = 0.011, (d) AuNP-100 at c_{AC}/c_{NP} = 0.0043 at the indicated temperature conditions. Solid curves denote theoretical values with the parameters listed in Table 2. Dashed lines, $S(q) = 1$.

The structure factor $S(q)$ with short-range attractive interactions between two spheres can be analyzed by the sticky hard sphere (SHS) model,[32-34] in which the well-like potential is used instead of the Lennard-Jones 6-12 potential to solve $S(q)$ analytically. In this scheme, the pair potential $u(R)$, where R is the intersphere distance, is $u(R) = \infty$ for $R < \sigma_s$, $u(R) = u_0$ for $\sigma_s < R < \sigma_s + \Delta$, and $u(R) = 0$ for $R > \sigma_s + \Delta$. The resulting $S(q)$ is expressed as

$$S(q) = f(q, \phi_{NP}, \sigma_s, \Delta, u_0/k_B T) \quad (5)$$

where ϕ_{NP}, k_B, and T are the volume fraction of nanoparticles, the Boltzmann constant, and the absolute temperature, respectively. The explicit expression is shown in the Supporting information as eqs S3 – S11. Assuming that the SHS is applicable to the current AuNPs with a finite size distribution and $\sigma_s = 2\ R_m$, the theoretical $S(q)$ can be calculated with the three fitting parameters of u_0, Δ, and ϕ_{NP}.

Since the attractive interaction between AuNPs mainly affects the $S(q)$ of the first minimum at about 0.4 and 0.2 nm^{-1} and the next peak at about 0.8 and 0.4 nm^{-1} for AuNP-10 and AuNP-20, respectively, in Figure 4, a curve fitting procedure was employed to reproduce them quantitatively. The analysis was not applied to AuNP-50 and AuNP-100 due to the insignificant q dependence of $S(q)_{app}$. Although the resulting theoretical values in Figure 4 satisfactorily explain the experimental data at the above-mentioned minimum and peak, the discrepancy between the experimental and theoretical values becomes noticeable at the low q end. This is most likely because the SHS only considers the short-range interaction whereas AC has a longer chain length (~ 300 nm) compared with AuNPs as is depicted in our previous report for the SiNP-AC complex.[19] On the other hand, some discrepancy was also seen for the higher q range as shown in Figure 4b (and 5a and 5b). A similar discrepancy was also found in the $S(q)$ data for aggregation of SiNP and lysozyme.[35] It was suggested that this is likely due to the polydispersity of SiNP. If the size of AuNPs causes the difference in the interaction via AC, the discrepancy in this study may also be due to the polydispersity of AuNPs. It should be noted that we attempted to choose similar parameters from Δ and ϕ_{NP} for the same AuNPs to readily compare the values of u_0. The values of $-u_0/k_BT$ at T_{prep} = 50 °C are significantly larger than those at T_{prep} = 0 °C, indicating that the temperature or the conformation of AC, triple helix or single coil, when the two components are mixed, plays an important role for the

aggregating AuNPs. Another interesting point is that T_{meas} does not appreciably influence $-u_0/k_BT$. Although we cannot conclude the reason, it is suggested that the conformation of AC partial chains absorbed on AuNPs might not change with increasing temperature because of significant attractive interactions between AuNPs and AC, or the kinetically yielded aggregation structure of AuNPs is not affected by the conformational change of AC after complexation.

Curve fitting analysis was also examined for the isovolumetric mixture of AuNP-5 and AC solutions as shown in Figure S6, for which the negative ζ potential suggests that excess AuNPs may not form a complex with AC. The resulting parameters are listed in Table S1. The temperature dependence of the parameters is similar to that for AuNP-10 and AuNP-20 mentioned above, suggesting the same temperature-dependent complex formation, although it should be noted that the parameters are affected by the dispersed AuNPs.

A similar analysis was also examined for ζ = 0 mixtures shown in Figure 5. The theoretical values calculated with the SHS parameters in Table 2 successfully explain the experimental data. The number of AuNPs in each droplet with a diameter of 1 μm can be roughly calculated to be on the order of 10^3 to 10^5, assuming that ϕ_{NP} reflects the volume fraction of AuNPs in the droplet. The resulting SHS parameters also show a similar tendency, while the T_{prep} dependence is less significant than that for the isovolumetric mixture. The reason will be discussed below with the data for UV-vis absorption.

Table 2. SHS Model Parameters for AuNPs with AC

Sample	c_{AC}/c_{NP}	ζ / mV	T_{prep} / °C	T_{meas} / °C	$-u_0 / k_BT$	Δ / nm	ϕ_{NP}
AuNP-10	0.165	11	50	15	1.4	1.8	0.12
			50	50	1.3	1.8	0.12
			0	50	0.2	2.1	0.11
			0	15	0.4	2.2	0.08
AuNP-20	0.188	13	50	15	1.6	1.0	0.20
			50	50	1.5	1.0	0.20
			0	50	0.8	1.0	0.17
			0	15	0.6	1.0	0.17
AuNP-10’	0.067	~ 0	50	15	1.0	1.3	0.14
			50	50	0.7	1.3	0.14
			0	50	0.6	1.3	0.14
			0	15	0.5	1.0	0.14
AuNP-20	0.030	~ 0	50	15	1.9	1.3	0.18
			50	50	1.9	1.3	0.18
			0	50	1.5	2	0.18
			0	15	1.3	2	0.18
AuNP-50	0.0092	~ 0	50	15	1.7	0.8	0.30
			50	50	1.7	0.8	0.30
			0	50	1.4	0.8	0.30
			0	15	1.0	1.0	0.30

UV-Vis Absorption. Since AuNPs have a surface plasmon resonance (SPR) band depending on AuNP size and aggregation, UV-vis spectra for AuNP-AC mixed solution reflect the complex formation, especially for the spatial arrangement of AuNPs. Therefore, Figure 6 shows the UV-vis spectra for AuNPs with or without AC. It should be noted that the extinction

coefficients on the vertical axis were calculated by using the mass concentration of AuNPs. The peak position for the AuNPs without AC tends to increase with the diameter; it should be noted that the data are essentially independent of the temperature between 15 and 50 °C. This is reasonable because the AuNPs are most perfectly dispersed in the buffer solution without AC. The peak position was red-shifted for the isovolumetric mixtures of AC and AuNPs at both low and high T_{meas} and T_{prep} (blue and red curves), indicating complex formation with AuNPs by AC molecules. The peak position at higher T_{prep} is appreciably higher than that at lower T_{prep} for AuNP-20, probably indicating more densely packed AuNPs in the AuNP-AC complex, while T_{prep} is insignificant for the other AuNPs. It is uncertain at this time whether the UV-vis absorption behavior is simply size-dependent. Considering that the formed AuNP-AC complex becomes larger in size and the dispersibility is not very stable as shown above in the SAXS section, some more experimental techniques can be developed to evaluate accurate spectra to reflect the aggregation structure properly. On the other hand, the peak wavelength for the mixtures of lower c_{AC}/c_{NP}, $\zeta = 0$ mixtures, is further red-shifted except for AuNP-100, suggesting a denser packing of AuNPs. Another interesting point is that the double peak was evaluated for AuNP-20 and AuNP-50, and the high absorption was maintained even at high λ_0 for AuNP-100, indicating that both dispersed AuNPs and densely packed AuNPs are present in the mixed solution because not all AuNPs can form a complex with AC.

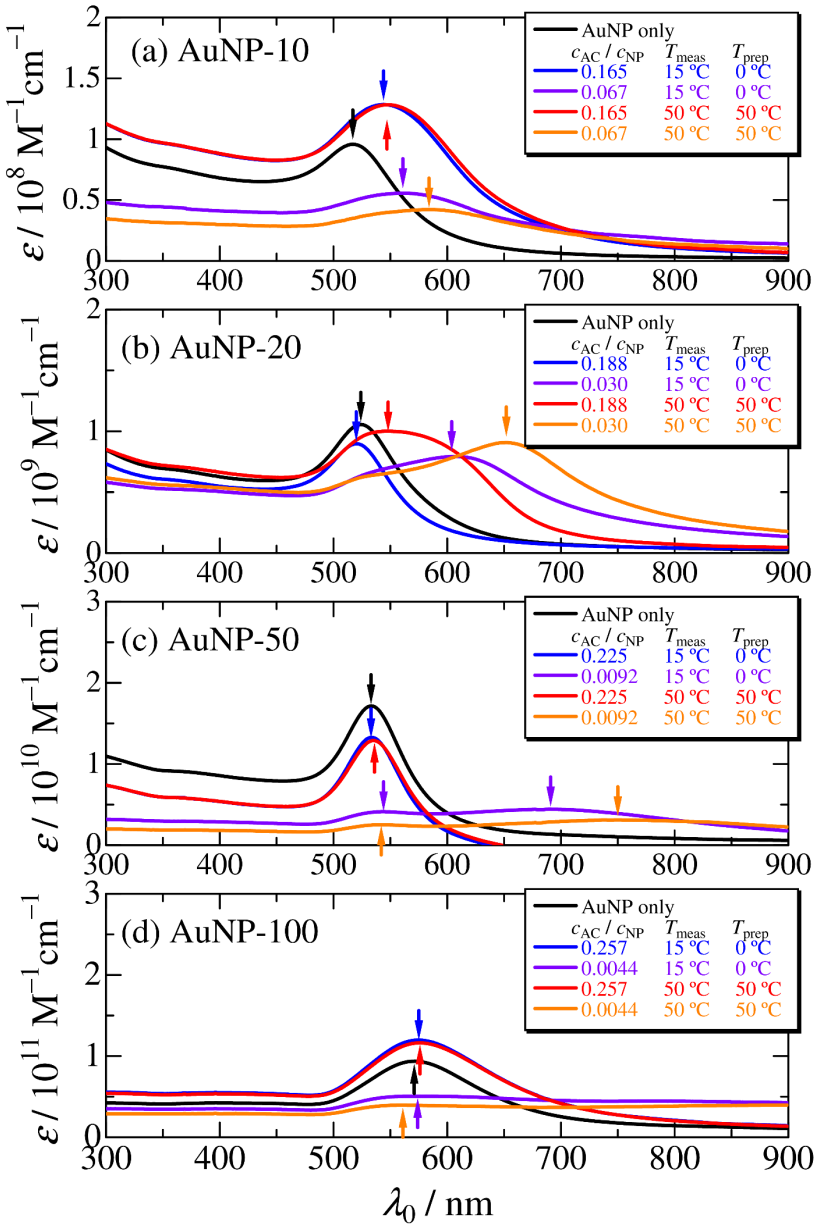

Figure 6. UV-VIS spectra for the mixed solutions of AC (c_{AC} = 1.0 × 10^{-2} mg/mL) in acetate buffer (50 mM, pH = 4) and AuNPs in 0.1 mM phosphate-buffered saline at 25 °C. (a) AuNP-10, (b) AuNP-20, (c) AuNP-50, (d) AuNP-100 with or without AC at the indicated c_{AC}/c_{NP} and temperatures.

Aggregation Structure. The evaluated structural features of the AuNP and AC complexes at different T_{prep} and mixing ratios are shown in Figure 7. As shown by xSight

measurements, micrometer-sized droplets were observed for all AuNP and AC mixtures investigated. Not a small number of the AuNPs are contained in the large droplet. This is supported by the fact that the $S(q)_{app}$ values did not converge to unity even at the high q end as described above. While no significant differences were observed in the micrometer droplet measurements, significant differences were observed in the SAXS profiles and absorption spectra. This means that at least at the nanoscale, the aggregation structure is influenced by the size of the AuNP, the mixing ratio, and the T_{prep}. Thus, the nanoscale aggregation structure is shown in the left part of the figure. For the isovolumetric mixture with positive ζ potential, the UV spectra are similar or slightly red-shifted compared to those for pure AuNP solutions. The red shift is more pronounced at higher T_{prep}. This indicates that slightly denser aggregates were yielded for the higher T_{prep} mixture as shown in Figure 7(a). This is supported by the SHS parameters in Table 2 estimated from the SAXS results. A possible reason is that the higher flexibility and thinner main chain of the single-chain AC tend to form complexes with AuNP more easily than the thick and stiff triple-helical AC.

The red shift of the absorption spectra is more significant for the $\zeta = 0$ mixtures, especially at high T_{prep}, while some spectra are bimodal, indicating that part of the AuNPs are not strongly complexed with AC as shown in Figure 7(b). This may affect the $S(q)_{app}$ data in Figure 5 and the resulting interaction parameters listed in Table 2. In other words, the evaluated SHS parameters for $\zeta = 0$ mixtures reflect the average interactions of densely packed and dispersed AuNPs. Another important point is that the disappeared ζ potential for AuNP-AC at a certain c_{AC}/c_{NP} indicates electrophilic neutralization at the mixing ratio. The bimodal UV-vis absorption indicates the existence of strongly associated and loosely associated AuNPs, which probably surround the vicinity of the aggregate by the electrostatic attractive interactions. The present result applies only to the interaction between AuNPs and enzymatically modified collagen. However, the resulting properties of the complex may play an important role in

elucidating intermolecular interactions between biopolymers and AuNPs, since AuNPs are widely used for biochemical applications as mentioned in the Introduction.

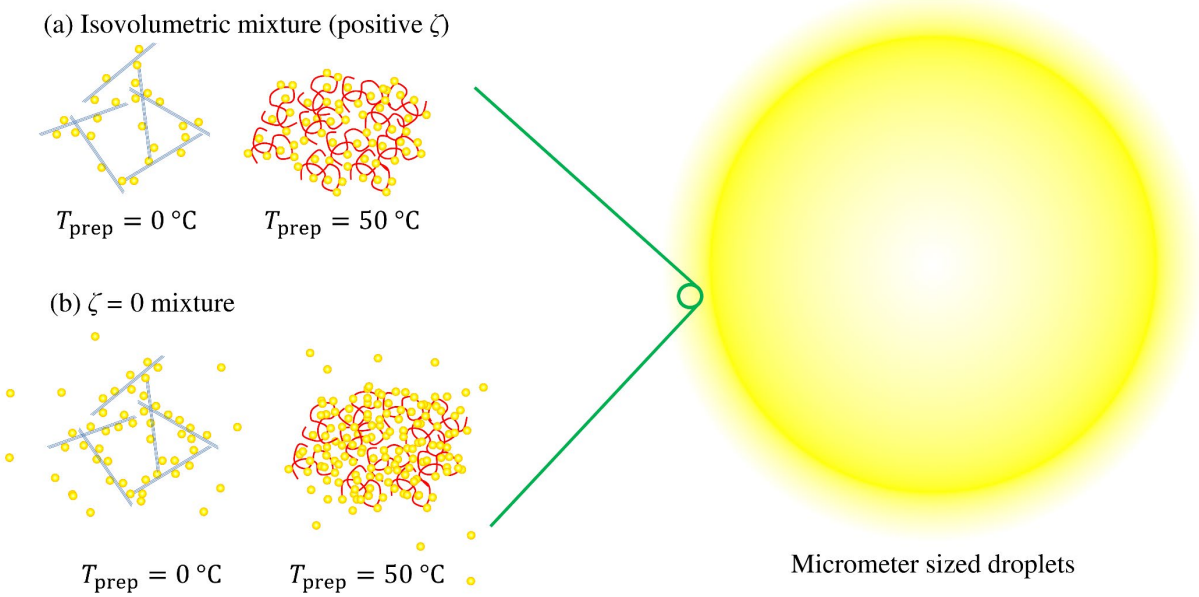

Figure 7. Schematic representation of AuNP and AC complex formation for (a) isovolumetric mixtures with positive ζ potential and (b) ζ = 0 mixtures in the pH = 4 buffer at different T_{prep}. Circles, AuNPs; blue lines, triple helical AC; red curves, single chain AC.

CONCLUSIONS

Significant complex formation was found for negatively charged gold nanoparticles (AuNPs) with AC in acetate buffer (pH 4) for both positive ζ and $\zeta = 0$ mixtures. The structure factor $S(q)$ of AuNPs with diameters between 10 and 100 nm showed that the complexation of AuNPs is more pronounced for smaller AuNPs, suggesting that the size-dependent surface area plays an important role in the complexation. The aggregation behavior can also be detected by the difference in surface plasmon absorption difference of AuNPs with or without AC. Another

important point is that the preparation temperature of the mixed solution of AuNPs and AC significantly affects the resulting aggregation structure, suggesting that the conformation of collagen in the mixing process determines the aggregation structure of AuNPs. A split absorption band was observed for $\zeta = 0$ mixtures, indicating that not all AuNPs form a tightly condensed complex with AC.

ASSOCIATED CONTENT

Supporting Information

The Supporting Information is available free of charge athttps://pubs.acs.org/doi/10.1021/…..

Results of total holographic characterization of the mixed solutions of AuNP and AC, SAXS profiles of AuNPs in acetate buffer and AuNP-5 with or without AC in acetate buffer, estimation of scattering intensity of AuNP and AC, explicit expression of eq 5, and structure factor of AuNP-5 with AC and the resulting SHS parameters (PDF).

ACKNOWLEDGEMENTS

The authors are grateful to Professor Emeritus Kazuo Sakurai (University of Kitakyushu) for the xSight measurement and Dr. Noboru Ohta (SPring-8) for the SAXS measurement. The synchrotron radiation experiments were performed at BL40B2 in SPring-8 under the approval of the Japan Synchrotron Radiation Research Institute (JASRI) (Proposal Nos. 2020A0529, 2021B1138, 2021B1139, 2022A1083, and 2022B1119). The xSight measurement was carried out at the Instrumentation Center, the University of Kitakyushu. This work was supported in part by JSPS KAKENHI Grant Numbers JP20H02788 and JP23H02011 and MEXT Promotion of Distinctive Joint Research Center Program Grant Number #JPMXP 0621467946.

References

1. Giljohann, D. A.; Seferos, D. S.; Daniel, W. L.; Massich, M. D.; Patel, P. C.; Mirkin, C. A., Gold nanoparticles for biology and medicine. *Angew. Chem. Int. Ed. Engl.* **2010,** *49* (19), 3280-94.
2. Das, M.; Shim, K. H.; An, S. S. A.; Yi, D. K., Review on gold nanoparticles and their applications. *Toxicology and Environmental Health Sciences* **2012,** *3* (4), 193-205.
3. Dreaden, E. C.; Alkilany, A. M.; Huang, X.; Murphy, C. J.; El-Sayed, M. A., The golden age: gold nanoparticles for biomedicine. *Chem. Soc. Rev.* **2012,** *41* (7), 2740-79.
4. Dykman, L.; Khlebtsov, N., Gold nanoparticles in biomedical applications: recent advances and perspectives. *Chem. Soc. Rev.* **2012,** *41* (6), 2256-82.
5. Yeh, Y. C.; Creran, B.; Rotello, V. M., Gold nanoparticles: preparation, properties, and applications in bionanotechnology. *Nanoscale* **2012,** *4* (6), 1871-80.
6. Eivazzadeh-Keihan, R.; Saadatidizaji, Z.; Mahdavi, M.; Maleki, A.; Irani, M.; Zare, I., Recent advances in gold nanoparticles-based biosensors for tuberculosis determination. *Talanta* **2024,** *275*, 126099.
7. Daems, N.; Michiels, C.; Lucas, S.; Baatout, S.; Aerts, A., Gold nanoparticles meet medical radionuclides. *Nucl Med Biol* **2021,** *100-101*, 61-90.
8. Roller, E. M.; Khorashad, L. K.; Fedoruk, M.; Schreiber, R.; Govorov, A. O.; Liedl, T., DNA-assembled nanoparticle rings exhibit electric and magnetic resonances at visible frequencies. *Nano Lett.* **2015,** *15* (2), 1368-73.
9. Gür, F. N.; Schwarz, F. W.; Ye, J.; Diez, S.; Schmidt, T. L., Toward Self-Assembled Plasmonic Devices: High-Yield Arrangement of Gold Nanoparticles on DNA Origami Templates. *ACS Nano* **2016,** *10* (5), 5374-5382.
10. Harimech, P. K.; Gerrard, S. R.; El-Sagheer, A. H.; Brown, T.; Kanaras, A. G., Reversible Ligation of Programmed DNA-Gold Nanoparticle Assemblies. *J. Am. Chem. Soc.* **2015,** *137* (29), 9242-5.
11. Okyem, S.; Awotunde, O.; Ogunlusi, T.; Riley, M. B.; Driskell, J. D., Probing the Mechanism of Antibody-Triggered Aggregation of Gold Nanoparticles. *Langmuir* **2021,** *37* (9), 2993-3000.
12. Charbgoo, F.; Nejabat, M.; Abnous, K.; Soltani, F.; Taghdisi, S. M.; Alibolandi, M.; Thomas Shier, W.; Steele, T. W. J.; Ramezani, M., Gold nanoparticle should understand protein corona for being a clinical nanomaterial. *J Control Release* **2018,** *272*, 39-53.
13. Liu, J.; Peng, Q., Protein-gold nanoparticle interactions and their possible impact on biomedical applications. *Acta Biomater* **2017,** *55*, 13-27.
14. Sanpui, P.; Paul, A.; Chattopadhyay, A., Theranostic potential of gold nanoparticle-protein agglomerates. *Nanoscale* **2015,** *7* (44), 18411-23.
15. Spadavecchia, J.; Apchain, E.; Alberic, M.; Fontan, E.; Reiche, I., One-step synthesis of collagen hybrid gold nanoparticles and formation on Egyptian-like gold-plated archaeological ivory. *Angew. Chem. Int. Ed. Engl.* **2014,** *53* (32), 8363-6.
16. Marisca, O. T.; Leopold, N., Anisotropic Gold Nanoparticle-Cell Interactions Mediated by Collagen. *Materials (Basel)* **2019,** *12* (7), 1131.
17. Zhao, Y.; Hu, W.; Kang, J.; Lin, X.; Wei, B.; Zhang, J.; Xu, C.; Wang, H., Monitoring fiber-like aggregation of collagen using gold nanoparticles as probes. *Chemical Papers* **2021,** *76* (3), 1377-1384.
18. Tang, M.; Gandhi, N. S.; Burrage, K.; Gu, Y., Interaction of gold nanosurfaces/nanoparticles with collagen-like peptides. *Phys. Chem. Chem. Phys.* **2019,** *21* (7), 3701-3711.

19. Terao, K.; Otsubo, M.; Abe, M., Complex Formation of Silica Nanoparticles with Collagen: Effects of the Conformation of Collagen. *Langmuir* **2020,** *36* (47), 14425-14431.
20. Otsubo, M.; Terao, K., Kinetics of the complex formation of silica nanoparticles with collagen. *Polym. J.* **2021,** *53* (12), 1481-1484.
21. Tomofuji, Y.; Terao, K., Complex Formation Behavior of Silica Nanoparticles and Xanthan. *Macromolecular Symposia* **2023,** *408* (1), 2200025.
22. Tomofuji, Y.; Matsuo, K.; Terao, K., Kinetics of denaturation and renaturation processes of double-stranded helical polysaccharide, xanthan in aqueous sodium chloride. *Carbohydr. Polym.* **2022,** *275*, 118681.
23. Stenzel, K. H.; Miyata, T.; Rubin, A. L., Collagen as a biomaterial. *Annu Rev Biophys Bioeng* **1974,** *3* (0), 231-53.
24. Wang, C.; Zhong, X.; Ruffner, D. B.; Stutt, A.; Philips, L. A.; Ward, M. D.; Grier, D. G., Holographic Characterization of Protein Aggregates. *J. Pharm. Sci.* **2016,** *105* (3), 1074-85.
25. Ueno, K.; Ueno, H.; Sato, T., Colloidal polyion complexation from sodium poly(acrylate) and poly(vinyl ammonium) chloride in aqueous solution. *Polym. J.* **2012,** *44* (1), 59-64.
26. Liu, H. D.; Sato, T., Polymer colloids formed by polyelectrolyte complexation of vinyl polymers and polysaccharides in aqueous solution. *Chin. J. Polym. Sci.* **2013,** *31* (1), 39-49.
27. Glatter, O.; Kratky, O., *Small Angle X-ray Scattering*. Academic Press: London, 1982.
28. Nakamura, Y.; Norisuye, T., Scattering function for wormlike chains with finite thickness. *Journal of Polymer Science Part B-Polymer Physics* **2004,** *42* (8), 1398-1407.
29. Yamakawa, H.; Yoshizaki, T., *Helical Wormlike Chains in Polymer Solutions, 2nd ed.* Springer: Berlin, Germany, 2016.
30. Nakamura, Y.; Norisuye, T., Brush-like polymers. In *Soft Matter Characterization*, Borsali, R.; Pecora, R., Eds. Springer Netherlands: 2008; pp 235-286.
31. Terao, K.; Mizuno, K.; Murashima, M.; Kita, Y.; Hongo, C.; Okuyama, K.; Norisuye, T.; Bächinger, H. P., Chain dimensions and hydration behavior of collagen model peptides in aqueous solution: [Glycyl-4(R)-hydroxyprolyl-4(R)-hydroxyproline](n), [glycylprolyl-4(R)-hydroxyproline](n), and some related model peptides. *Macromolecules* **2008,** *41* (19), 7203-7210.
32. Baxter, R. J., Percus-Yevick Equation for Hard Spheres with Surface Adhesion. *J. Chem. Phys.* **1968,** *49* (6), 2770-2774.
33. Menon, S. V. G.; Manohar, C.; Rao, K. S., A New Interpretation of the Sticky Hard-Sphere Model. *J. Chem. Phys.* **1991,** *95* (12), 9186-9190.
34. Hashimoto, T., *Principles and Applications of X-ray, Light and Neutron Scattering*. 2022; p 1-627.
35. Bharti, B.; Meissner, J.; Findenegg, G. H., Aggregation of silica nanoparticles directed by adsorption of lysozyme. *Langmuir* **2011,** *27* (16), 9823-33.

For Table of Contents Use Only

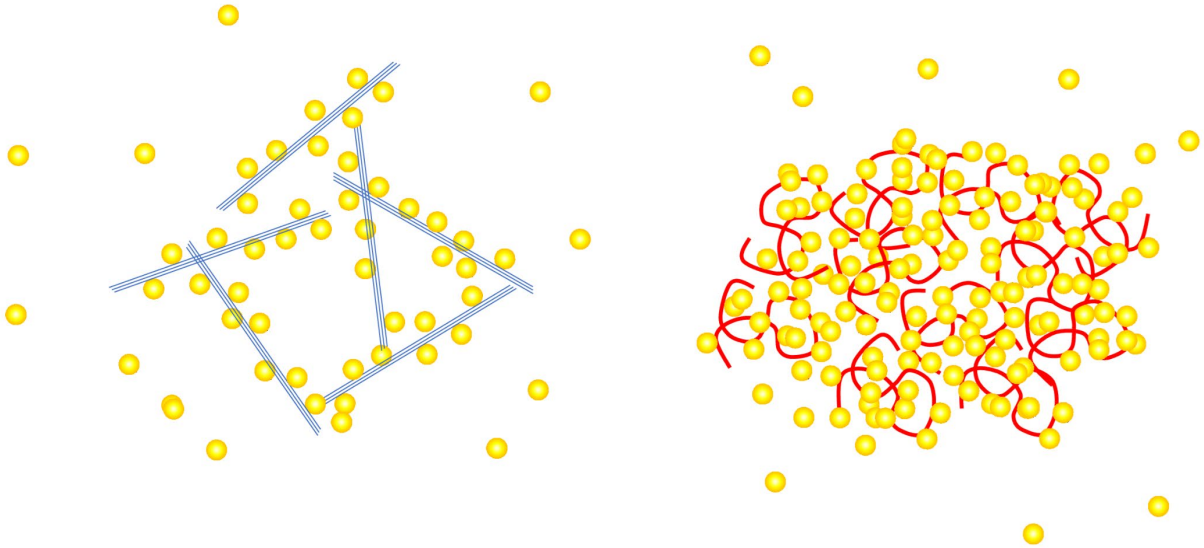

Supporting Information for

Complex Formation of Gold Nanoparticles with Collagen in Aqueous Media Studied by X-ray Scattering and Absorption Spectroscopy

Kota Sagawa and Ken Terao*

Department of Macromolecular Science, Graduate School of Science, Osaka University, 1-1, Machikaneyama-cho, Toyonaka, Osaka 560-0043, Japan.

* Corresponding author. E-mail address: terao.ken.sci@osaka-u.ac.jp

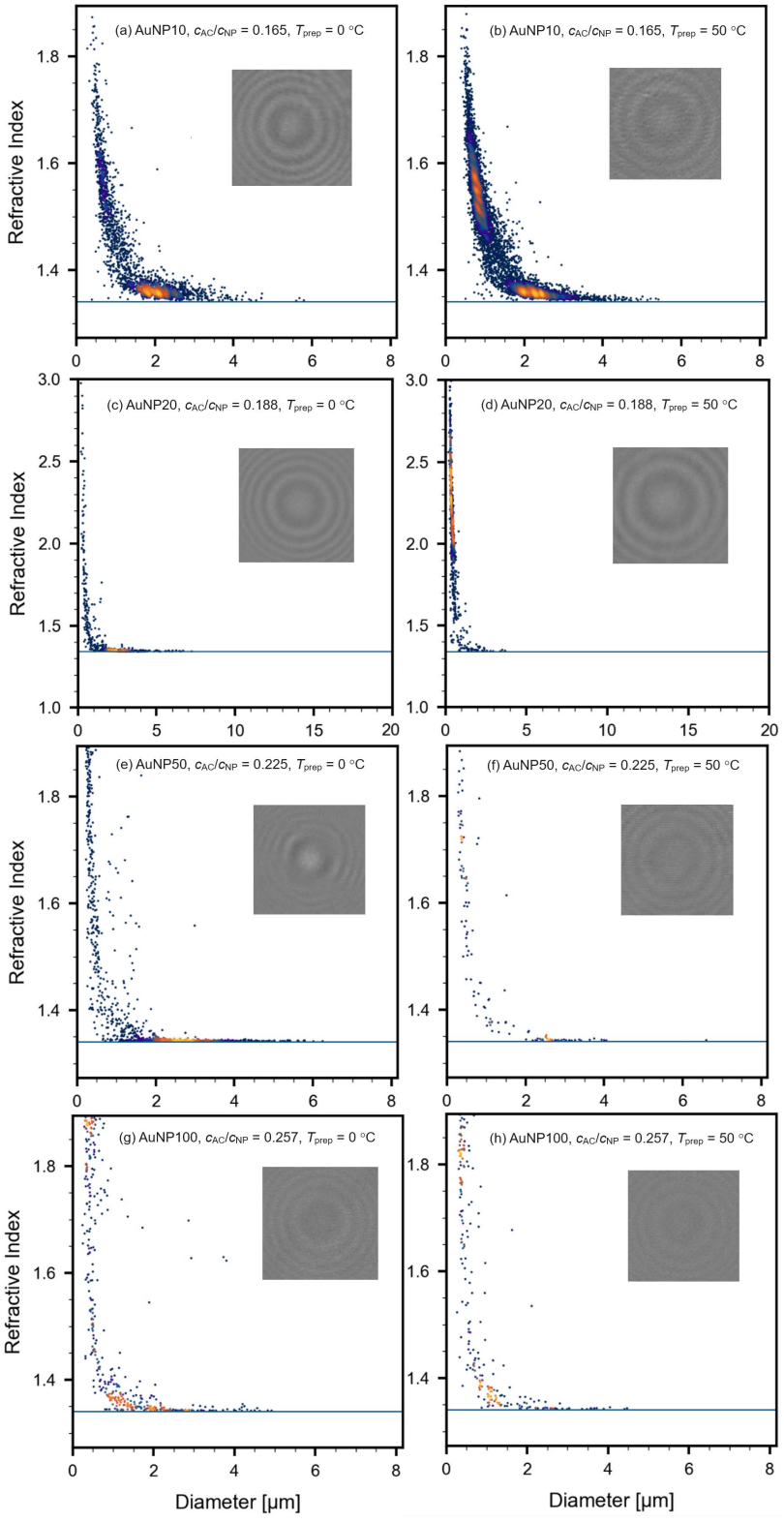

Figure S1. Results of the xSight measurements for isovolumetric mixed solutions at 25 °C. Relationship between refractive index and diameter of the indicated AuNP and at the indicated T_{prep}. Inset is an example of the scattering pattern of a particle.

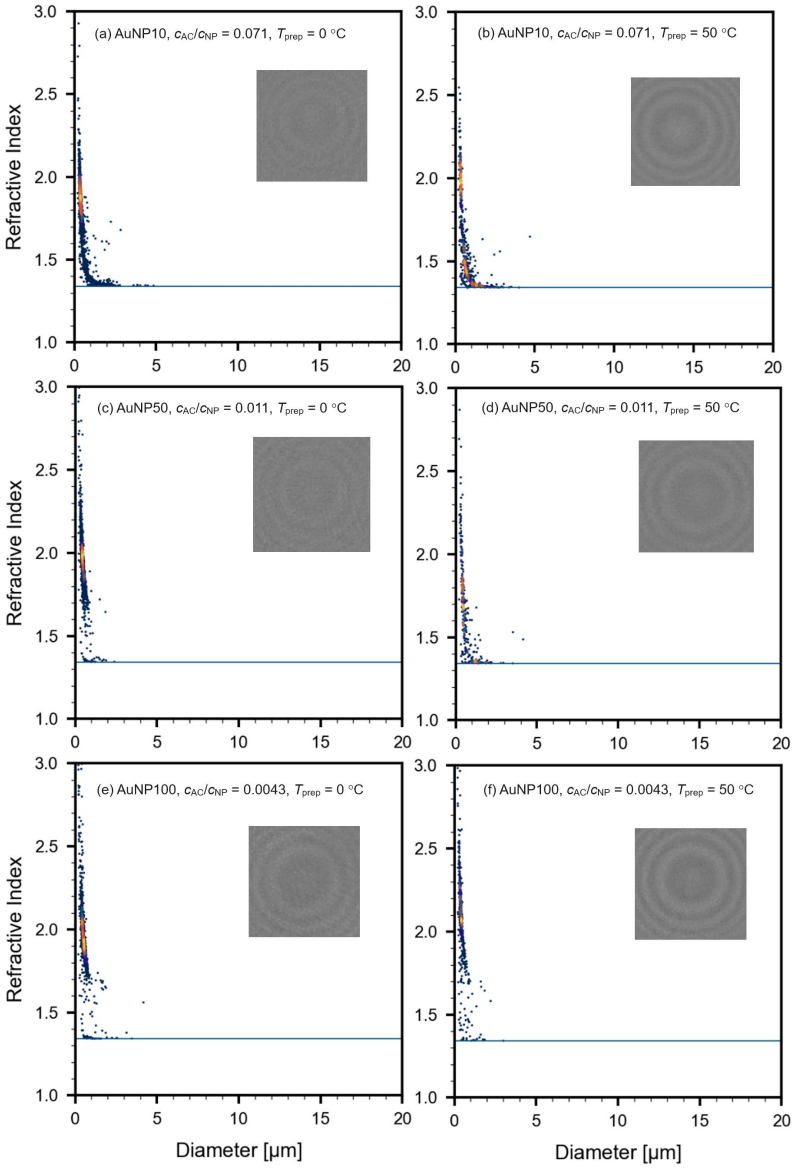

Figure S2. Results of the xSight measurements for $\zeta = 0$ mixtures at 25 °C. Relationship between refractive index and diameter of the indicated AuNP and at the indicated T_{prep}. Inset is an example of the scattering pattern of a particle.

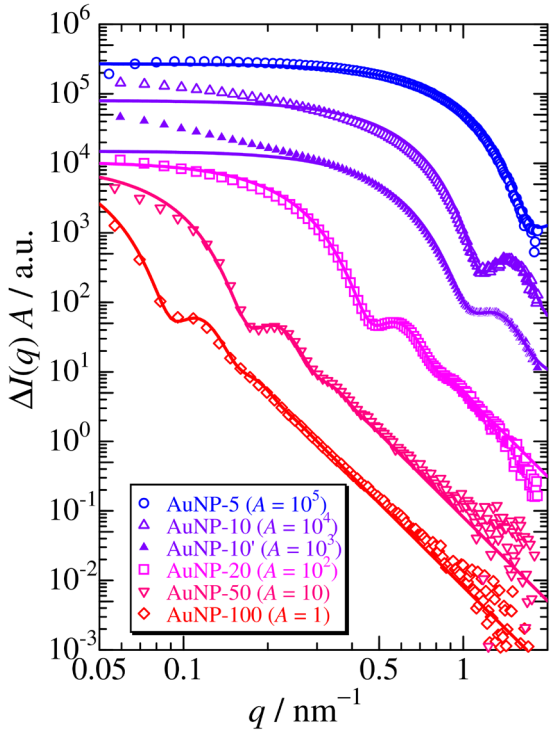

Figure S3. Double logarithmic plots for the excess scattering intensity $\Delta I(q)$ vs q for the isovolumetric mixture of the gold nanoparticles (AuNPs) in 0.1 mM phosphate buffered saline and 50 mM acetate buffer (pH = 4) at indicated temperature conditions at 15 °C.

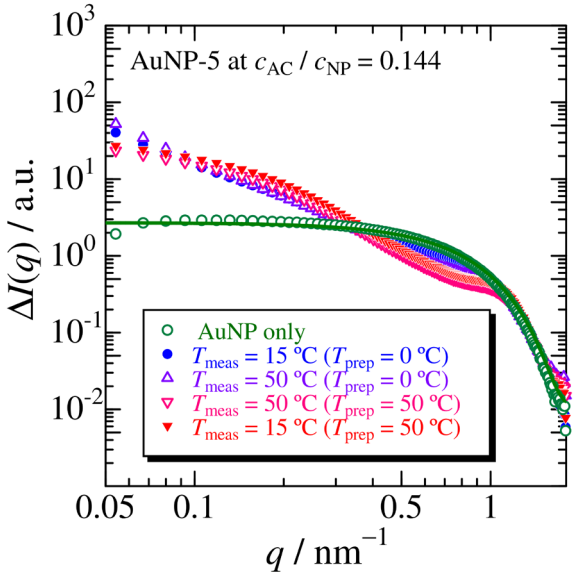

Figure S4. Double logarithmic plots of excess scattering intensity $\Delta I(q)$ vs. q for the isovolumetric mixture of AC ($c_{AC} = 1.0 \times 10^{-2}$ mg/mL) in acetate buffer (50 mM, pH = 4) and AuNP-5 in 0.1 mM phosphate buffered saline (at $c_{AC}/c_{NP} = 0.165$). The gold-only solution was prepared by isovolumetric mixing with 50 mM acetate buffer. Solid green curves indicate calculated values for polydisperse spheres (see Figure S3).

Estimation of the scattering intensity of goldnoparticles (AuNPs) and atelocollagen (AC). The excess scattering intensity $\Delta I(0)$ of the dilute solution is proportional to the square of the contrast factor Δz as[1]

$$\Delta I(0) \propto \Delta z^2 M c \qquad \text{(S1)}$$

$$\Delta z = z - \bar{v}\rho_{\mathrm{e,s}} \qquad \text{(S2)}$$

Here, M is the molar mass of the solute, c is the mass concentration, z is the number of moles of electrons per unit mass of the solute, $\bar{v}$ is the partial specific volume of the solute, and $\rho_{\mathrm{e,s}}$ is the electron density of the solvent. Assuming the bulk gold density (19.32 g mL^{-1}) for the gold particles, Δz for the AuNPs is estimated to be 0.372 mol/g, and M for AuNP-10 and AuNP-100 are calculated to be 2.9×10^3 kg mol^{-1} and 6.1×10^6 kg mol^{-1}, respectively, from the mean diameter. The calculated $\Delta z^2 MP(q)/c$ for AuNP-5 and AuNP-100 are shown in Figure S1. The value for the triple helical AC can be calculated using Δz for a collagen model peptide,[2] M = 300 kg mol^{-1}, and the completely rodlike conformation for which $P(q)$ can be calculated[3] by the length L = 300 nm and the diameter of 1.6 nm.[2] The $\Delta z^2 MP(q)/c$ value for single chain AC can be calculated with M = 100 kg mol^{-1} and $P(q)$ for the wormlike cylinder model[4, 5] with the contour length L = 300 nm, the Kuhn segment length λ^{-1} = 3 nm (the chain stiffness),[2] and the chain diameter d = 0.5 nm.[2] The calculated values for AC are also shown in Figure S1.

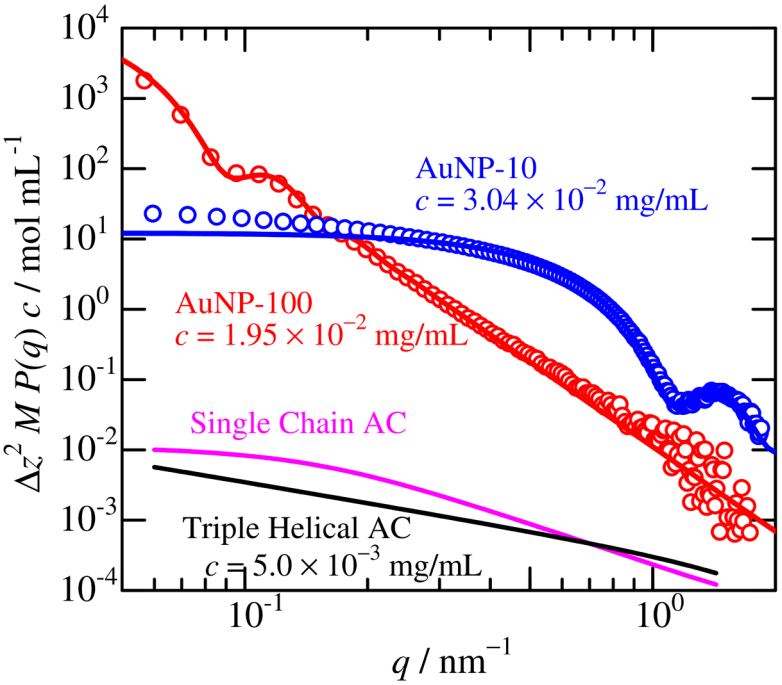

Figure S5. Absolute SAXS scattering intensity $\Delta z^2 MP(q)c$ for AuNP-10, AuNP-100, single chain AC, and triple helical AC.

Explicit expression of eq 5. According to the theory,[6-8] equation 5 in the main text is expressed as follows.

$$S(q) = f(q, \phi_{\mathrm{NP}}, \sigma_{\mathrm{s}}, \Delta, u_0/k_{\mathrm{B}}T) = [A^2(q) + B^2(q)]^{-1} \tag{S3}$$

$$A(q) = 1 + 12\eta\left(\alpha_{\mathrm{a}}\frac{\sin U_{\mathrm{a}} - U_{\mathrm{a}}\cos U_{\mathrm{a}}}{{U_{\mathrm{a}}}^3} + \beta_{\mathrm{a}}\frac{1-\cos U_{\mathrm{a}}}{{U_{\mathrm{a}}}^2} - \frac{\lambda_{\mathrm{s}}}{12}\frac{\sin U_{\mathrm{a}}}{U_{\mathrm{a}}}\right) \tag{S4}$$

$$B(q) = 12\eta\left\{\alpha_{\mathrm{a}}\left(\frac{1}{2U_{\mathrm{a}}} - \frac{\sin U_{\mathrm{a}}}{{U_{\mathrm{a}}}^2} + \frac{1-\cos U_{\mathrm{a}}}{{U_{\mathrm{a}}}^3}\right) + \beta_{\mathrm{a}}\left(\frac{1}{U_{\mathrm{a}}} - \frac{\sin U_{\mathrm{a}}}{{U_{\mathrm{a}}}^2}\right) - \frac{\lambda_{\mathrm{s}}}{12}\frac{1-\cos U_{\mathrm{a}}}{U_{\mathrm{a}}}\right\} \tag{S5}$$

$$U_{\mathrm{a}} = q(\sigma_{\mathrm{s}} + \Delta) \tag{S6}$$

$$\alpha_{\mathrm{a}} = \frac{1-2\eta-\lambda_{\mathrm{s}}\eta(1-\eta)}{(1-\eta)^2} \tag{S7}$$

$$\beta_{\mathrm{a}} = \frac{-3\eta+\lambda_{\mathrm{s}}\eta(1-\eta)}{2(1-\eta)^2} \tag{S8}$$

$$\frac{\eta}{12}{\lambda_{\mathrm{s}}}^2 - \left(\tau + \frac{\eta}{1-\eta}\right)\lambda_{\mathrm{s}} + \frac{2+\eta}{2(1-\eta)^2} = 0 \tag{S9}$$

$$\tau = \frac{\sigma_{\mathrm{s}}+\Delta}{12\Delta}\exp\left(\frac{u_0}{k_{\mathrm{B}}T}\right) \tag{S10}$$

$$\eta = \left(\frac{\sigma_{\mathrm{s}}+\Delta}{\sigma_{\mathrm{S}}}\right)^3 \phi_{\mathrm{NP}} \tag{S11}$$

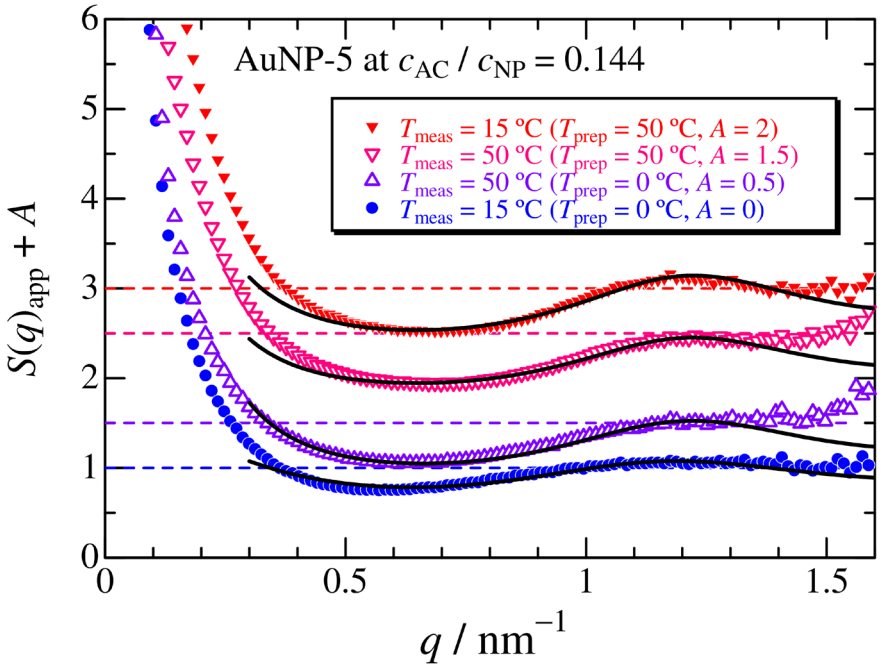

Figure S6. Plots of $S(q)$ vs q estimated from the data in Figure S5 at the indicated temperature conditions. Solid curves denote theoretical values with the parameters listed in Table S1. Dashed lines, $S(q) = 1$.

Table S1. SHS Model Parameters for AuNP-5 with AC

Sample	c_{AC}/c_{NP}	ζ / mV	T_{prep} / °C	T_{meas} / °C	$-u_0$ / k_BT	Δ / nm	ϕ_{NP}
AuNP-5	0.144	−9	50	15	0.7	1.2	0.12
			50	50	0.7	1.2	0.12
			0	50	0.45 ± 0.05	1.2	0.12
			0	15	0.2	1.2	0.08

References

1. Glatter, O.; Kratky, O., *Small Angle X-ray Scattering*. Academic Press: London, 1982.

2. Terao, K.; Mizuno, K.; Murashima, M.; Kita, Y.; Hongo, C.; Okuyama, K.; Norisuye, T.; Bächinger, H. P., Chain dimensions and hydration behavior of collagen model peptides in aqueous solution: [Glycyl-4(R)-hydroxyprolyl-4(R)-hydroxyproline](n), [glycylprolyl-4(R)-hydroxyproline](n), and some related model peptides. *Macromolecules* **2008,** *41* (19), 7203-7210.

3. Nakamura, Y.; Norisuye, T., Scattering function for wormlike chains with finite thickness. *Journal of Polymer Science Part B-Polymer Physics* **2004,** *42* (8), 1398-1407.

4. Yamakawa, H.; Yoshizaki, T., *Helical Wormlike Chains in Polymer Solutions, 2nd ed.* Springer: Berlin, Germany, 2016.

5. Nakamura, Y.; Norisuye, T., Brush-like polymers. In *Soft Matter Characterization*, Borsali, R.; Pecora, R., Eds. Springer Netherlands: 2008; pp 235-286.

6. Baxter, R. J., Percus-Yevick Equation for Hard Spheres with Surface Adhesion. *J. Chem. Phys.* **1968,** *49* (6), 2770-2774.

7. Menon, S. V. G.; Manohar, C.; Rao, K. S., A New Interpretation of the Sticky Hard-Sphere Model. *J. Chem. Phys.* **1991,** *95* (12), 9186-9190.

8. Hashimoto, T., *Principles and Applications of X-ray, Light and Neutron Scattering*. 2022; p 1-627.